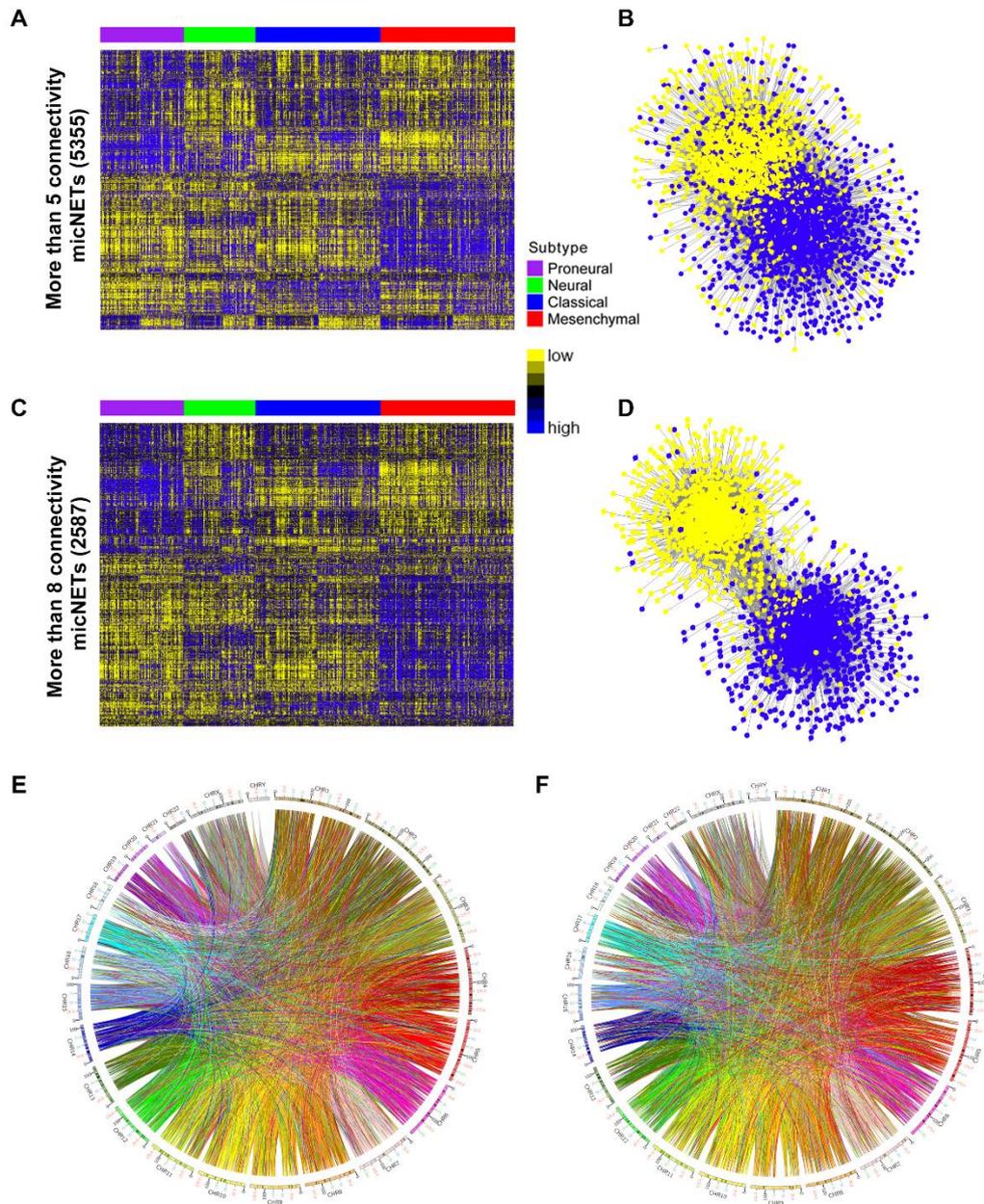Figure S1. The scheme of ceRNA network construction.

Figure S2. The ceRNA network based on the number of miRNAs shared between ceRNA pairs to eight and five, respectively. (A) Genes that interacted with each other in a ceRNA manner (> 5 connectivity) are presented in a cluster arranged according to proneural, neural, classical and mesenchymal subtypes. (B) The ceRNA genes (> 5 connectivity) formed a network in which the highly expressed micNETs in the mesenchymal subtype were labeled blue, whereas genes with low expression were labeled yellow. (C) Genes that interacted with each other in a ceRNA manner (> 8 connectivity) are presented in a cluster arranged according to proneural, neural, classical and mesenchymal subtypes. (D) The ceRNA genes (> 8 connectivity) formed a network in which the highly expressed micNETs in the mesenchymal subtype were labeled blue, whereas genes with low expression were labeled yellow. (E, F)

Genes in the ceRNA network were not enriched in specific chromosomes but rather were uniformly distributed throughout the genome.
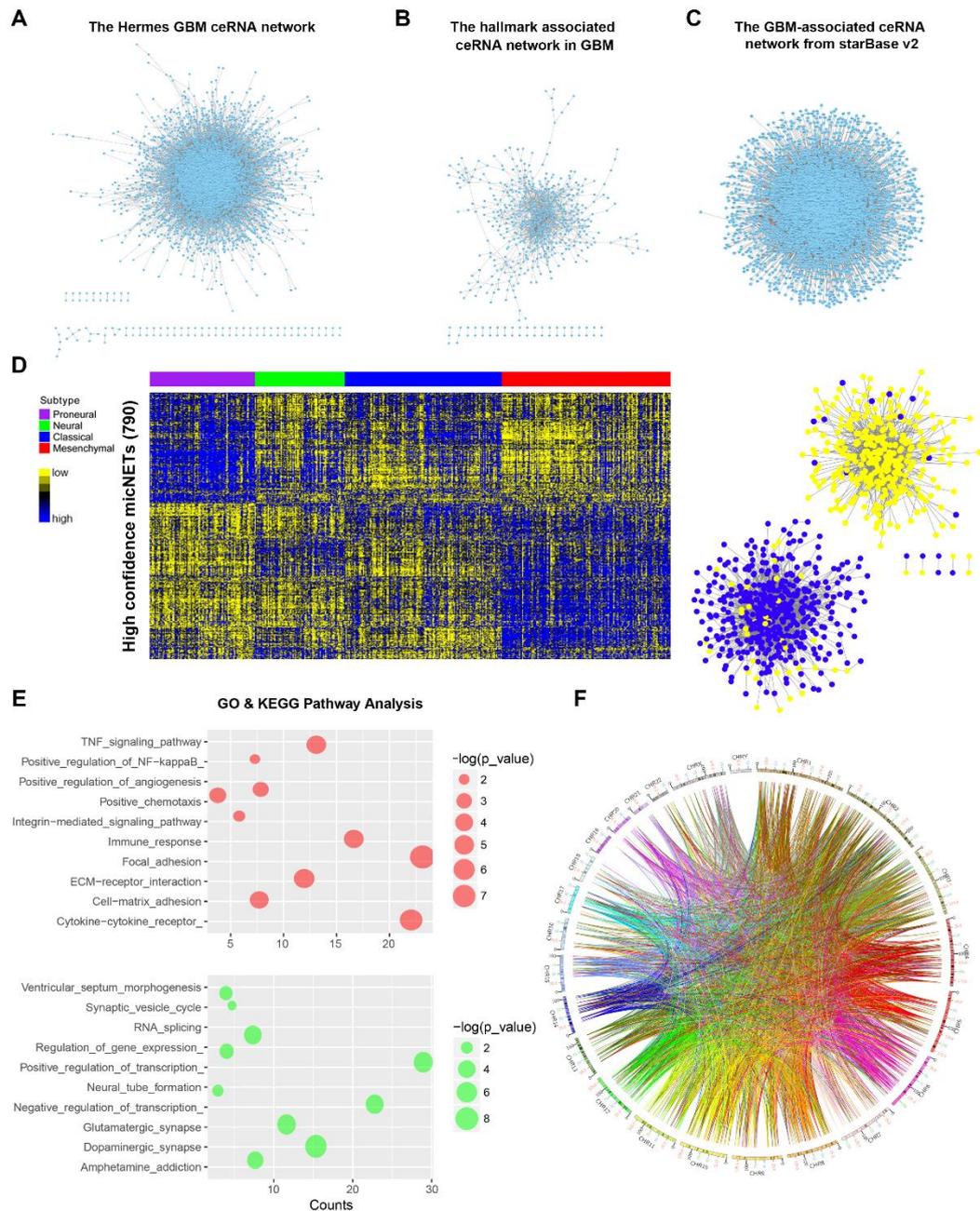

Figure S3. The high confidence ceRNA network from our ceRNA network by extracting connections in the three public ceRNA networks. (A) The Hermes GBM ceRNA network. (B) The hallmark associated ceRNA networks in 20 major cancers (including GBM). (C) The cancer-associated ceRNA networks from starBase v2. (D) The high confidence ceRNA network consists of two distinct subnetworks. (E) The subnetwork with genes highly expressed in the mesenchymal subtype was enriched in EMT-related pathways, whereas the subnetwork of lowly expressed genes was associated with proneural related functions. (F)

Genes in the ceRNA network were not enriched in specific chromosomes but rather were uniformly distributed throughout the genome.
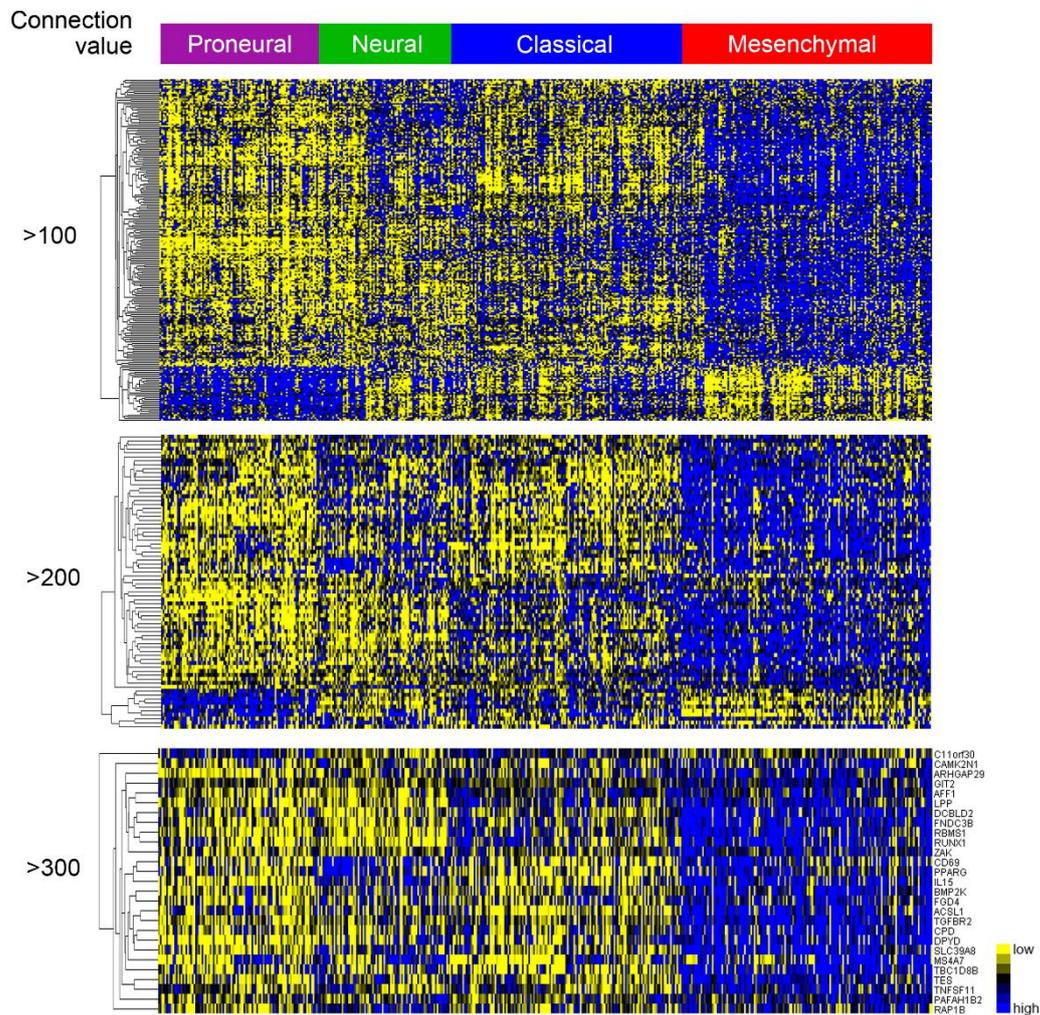

Figure S4. MicNETs with a high degree of connectivity tend to be enriched in the mesenchymal subtype. Heatmaps of ceRNA genes revealed the expression pattern of micNETs with more than 100 connections, more than 200 connections and more than 300 connections.
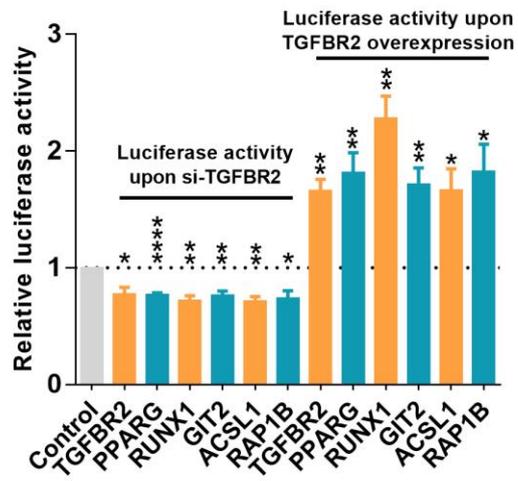
Figure S5. The 3'-UTR luciferase reporters' activity of TGFBR2, RUNX1, PPARG, GIT2, ACSL1 and RAP1B in glioma cells treated by TGFBR2 knockdown or overexpression.
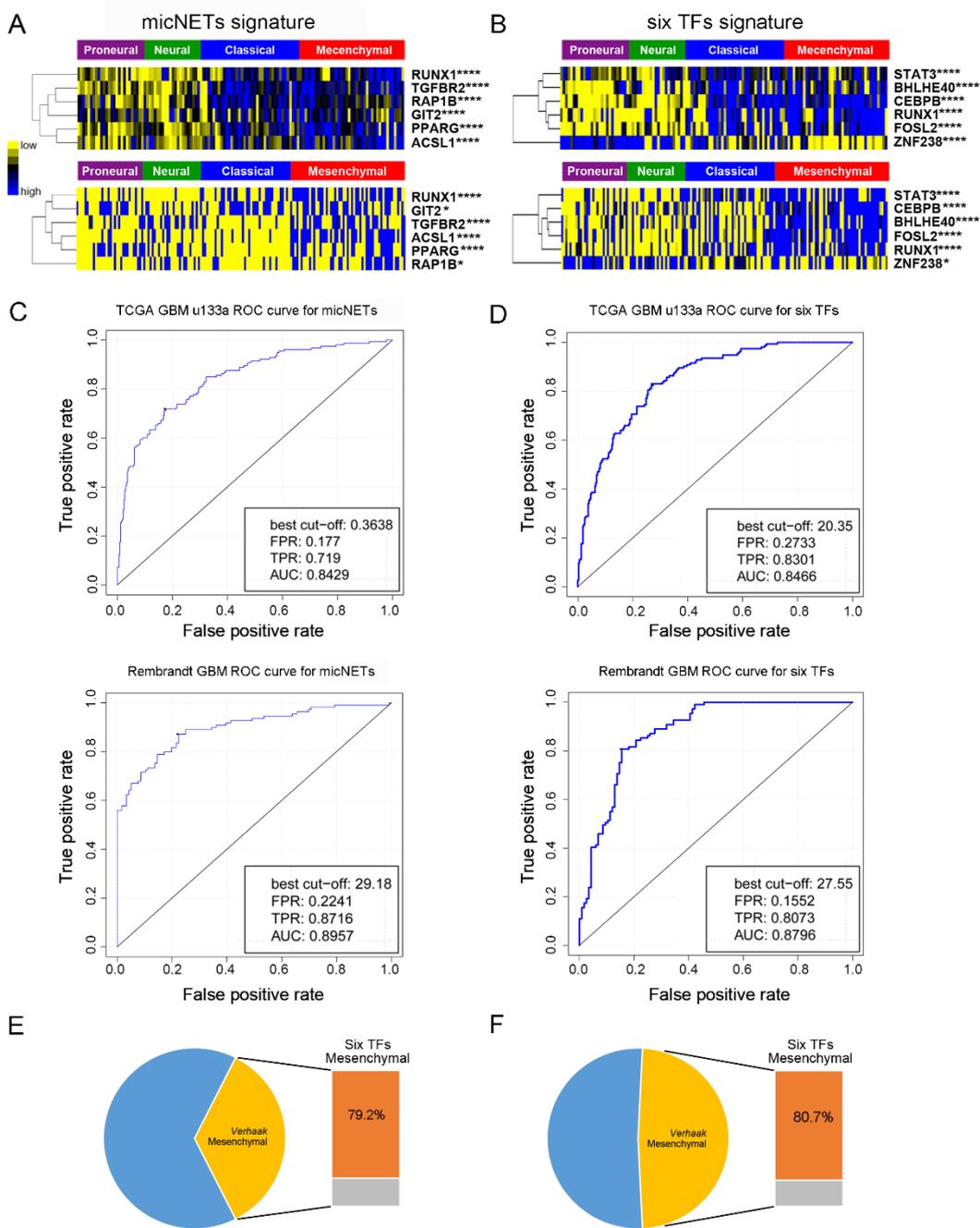
Figure S6. The expression levels of six micNETs predicted the mesenchymal subtype. (A) Heatmaps showing the six micNETs that were highly expressed in mesenchymal subtypes in the TCGA Agilent and u133a datasets. (B) Heatmaps showing the six TFs that were highly expressed in mesenchymal subtypes in the TCGA Agilent and u133a datasets. (C) ROC analysis revealed the predictive value of the micNETs signature for the mesenchymal subtype in the TCGA u133a and Rembrandt datasets. (D) ROC analysis revealed the predictive value of the six-TF signature for the mesenchymal subtype in the TCGA u133a and Rembrandt

datasets. (E, F) The frequency of mesenchymal samples predicted by the six-TF signature in Verhaak et al.'s mesenchymal subtype in the TCGA HiSeq and Rembrandt datasets.
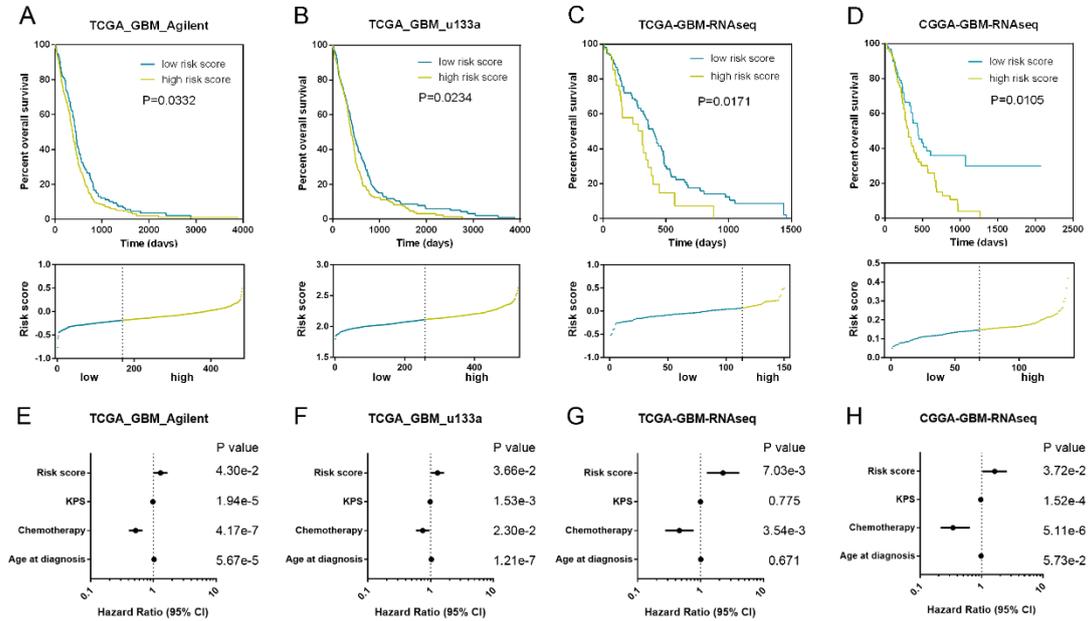

Figure S7. High risk score of micNETs predicts poor survival in patients with GBM. The overall survival of high risk scores and low risk scores of six micNETs were analyzed by Kaplan-Meier analysis in the TCGA Agilent (A), TCGA u133a (B), TCGA RNA-seq (C) and CGGA RNA-seq (D) databases. The distribution of risk score and corresponding cut off were shown. (E-H) Cox regression analysis was used to adjust for other factors associated with patient survival.
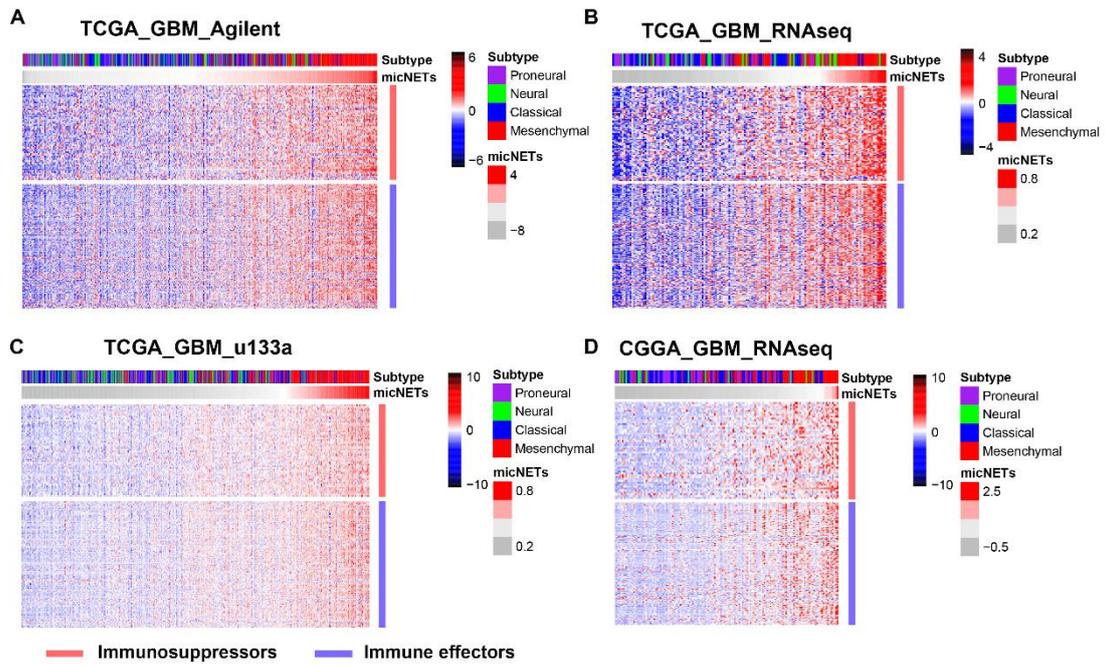
Figure S8. The proportion of patients with higher micNETs score had a significantly higher correlation with immunosuppressors and immune effectors in the TCGA and CGGA databases.
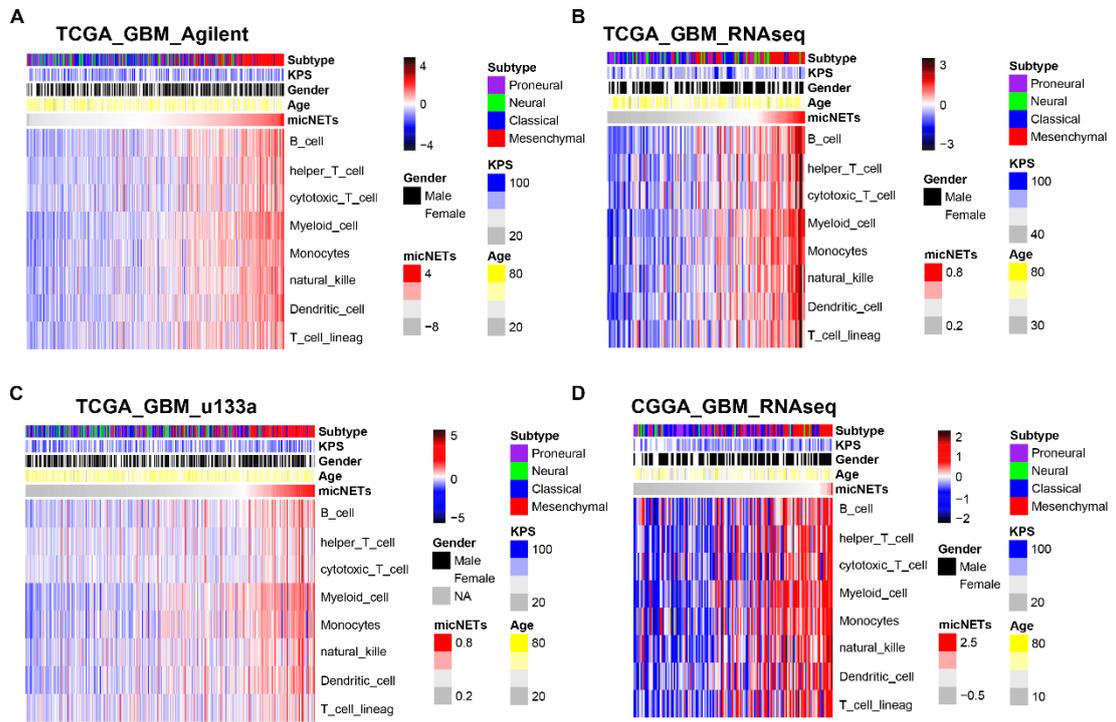
Figure S9. MicNETs score was positively associated with immune cell lineages, such as B cell, helper T cells, cytotoxic T cells, myeloid cells, monocytes, NK cells, dendritic cells and T-cell lineage in the TCGA and CGGA databases.
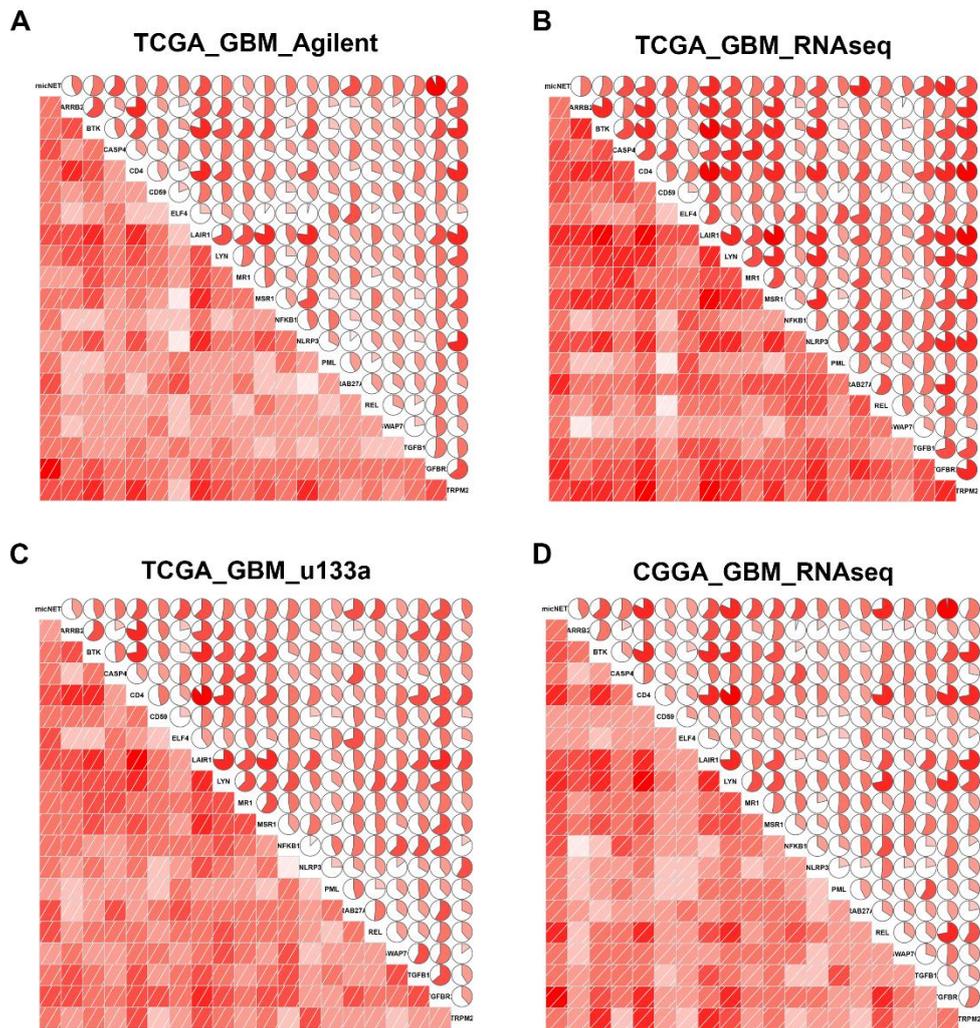
A TCGA_GBM_Agilent

B TCGA_GBM_RNAseq

C TCGA_GBM_u133a
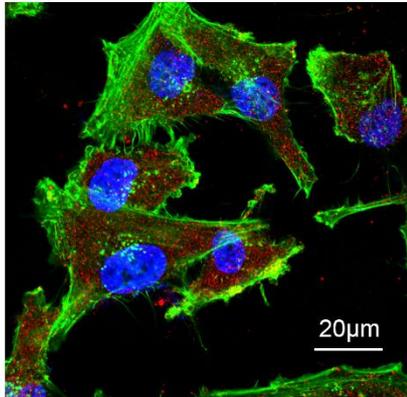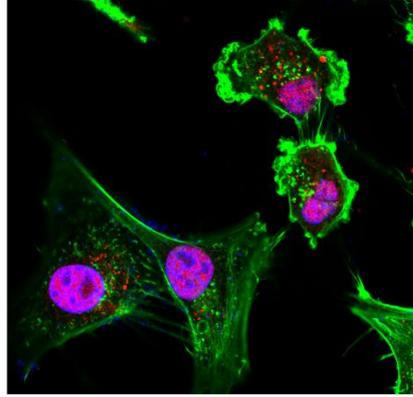
D CGGA_GBM_RNAseq

Figure S10. The six micNETs was significantly correlated with several immunosuppressors, such as ARRB2, BTK, CASP4, CD4, CD59, ELF4, LAIR1, LYN, MR1, MSR1, NFKB1, NLRP3, PML, RAB27A, REL, SWAP70, TGFB1, TGFBR2, TRPM2 in the TCGA and CGGA databases.
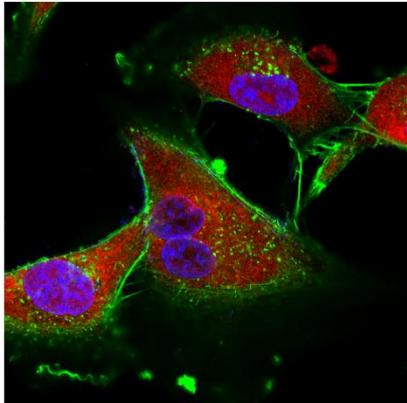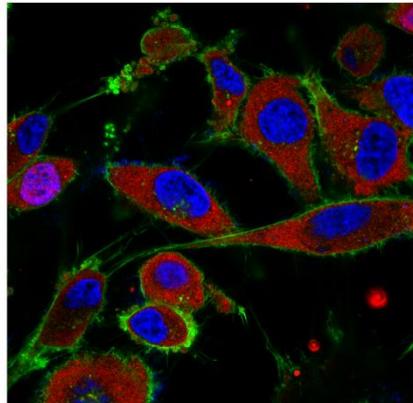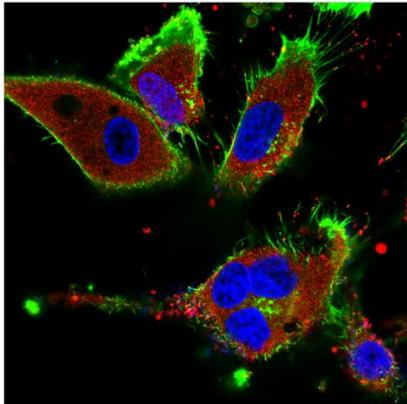
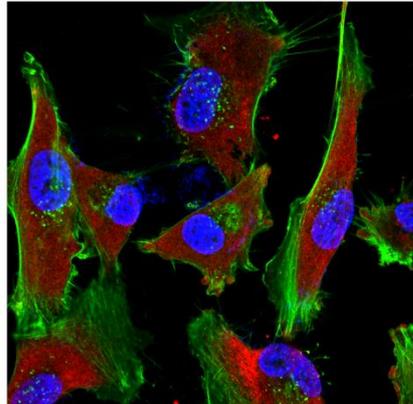TGFBR2/DAPI/F-actin

RUNX1

PPARG

GIT2

ACSL1

RAP1B

Figure S11. The immunofluorescence validated the micNETs protein subcellular localization in GBM cells.

Table S1. The TCGA subtype information in the enrolled public datasets.

Table S2. The differential genes (> 5 connectivity) in the ceRNA subnetworks.

Table S3. The differential genes (> 8 connectivity) in the ceRNA subnetworks.

Table S4. The differential genes (> 10 connectivity) in the ceRNA subnetworks.

Table S5. GO and KEGG Pathway analysis of genes in the upregulated ceRNA subnetwork.

Table S6. GO and KEGG Pathway analysis of genes in the downregulated ceRNA subnetwork.

Table S7. The high confidence ceRNA network.

Table S8. ClueGO analysis of the micNETs signature.

Table S9. ClueGO analysis of the "mesenchymal" genes targeted by six TFs.

Table S10. GO and KEGG Pathway analysis of the differentially expressed genes in PDX treated by DMSO and LY2109761.

Table S11. The gene list and membership in every clusters of Mfuzz.